Cancer Letters 375 (2016) 384–389

Contents lists available at ScienceDirect

Cancer Letters

journal homepage: www.elsevier.com/locate/canlet

Original Articles

Neuroblastoma patient-derived orthotopic xenografts reflect the microenvironmental hallmarks of aggressive patient tumours

Noémie Braekeveldt [a], Caroline Wigerup [a], Irene Tadeo [b], Siv Beckman [a], Caroline Sandén [c], Jimmie Jönsson [c], Jonas S. Erjefält [c], Ana P. Berbegall [b], Anna Börjesson [d], Torbjörn Backman [d], Ingrid Øra [e], Samuel Navarro [b], Rosa Noguera [b], David Gisselsson [f,g], Sven Påhlman [a], Daniel Bexell [a,*]

[a] Translational Cancer Research, Lund University, Lund, Sweden
[b] Department of Pathology, Medical School, University of Valencia-INCLIVA, Valencia, Spain
[c] Department of Experimental Medical Science, Lund University and Medetect AB, Lund, Sweden
[d] Department of Paediatric Surgery, Skåne University Hospital, Lund, Sweden
[e] Department of Paediatrics, Paediatric Oncology, Clinical Sciences, Lund University, Lund, Sweden
[f] Department of Clinical Genetics, Lund University, Lund, Sweden
[g] Department of Pathology, University and Regional Laboratories, Lund, Sweden

ARTICLE INFO

Article history:
Received 16 December 2015
Received in revised form 25 February 2016
Accepted 25 February 2016

Keywords:
Paediatric cancer
Neuroblastoma
Tumour microenvironment
Tumour stroma
Patient-derived xenograft (PDX)
Metastasis

ABSTRACT

Treatment of high-risk childhood neuroblastoma is a clinical challenge which has been hampered by a lack of reliable neuroblastoma mouse models for preclinical drug testing. We have previously established invasive and metastasising patient-derived orthotopic xenografts (PDXs) from high-risk neuroblastomas that retained the genotypes and phenotypes of patient tumours. Given the important role of the tumour microenvironment in tumour progression, metastasis, and treatment responses, here we analysed the tumour microenvironment of five neuroblastoma PDXs in detail. The PDXs resembled their parent tumours and retained important stromal hallmarks of aggressive lesions including rich blood and lymphatic vascularisation, pericyte coverage, high numbers of cancer-associated fibroblasts, tumour-associated macrophages, and extracellular matrix components. Patient-derived tumour endothelial cells occasionally formed blood vessels in PDXs; however, tumour stroma was, overall, of murine origin. Lymphoid cells and lymphatic endothelial cells were found in athymic nude mice but not in NSG mice; thus, the choice of mouse strain dictates tumour microenvironmental components. The murine tumour microenvironment of orthotopic neuroblastoma PDXs reflects important hallmarks of aggressive and metastatic clinical neuroblastomas. Neuroblastoma PDXs are clinically relevant models for preclinical drug testing.
© 2016 The Authors. Published by Elsevier Ireland Ltd. This is an open access article under the CC BY-NC-ND license (http://creativecommons.org/licenses/by-nc-nd/4.0/).

Introduction

The high attrition of novel agents hampers oncology drug development [1,2], in part because conventional preclinical cancer models do not fully resemble the clinical disease and thus have low predictive power [2–4]. Patient-derived xenografts (PDXs) have recently attracted interest because established PDXs faithfully reflect the genetic and histopathological characteristics of human disease. As a consequence, PDXs better predict clinical outcomes than conventional cell line-derived xenografts, and PDXs have emerged as a promising strategy to personalise patient selection and treatment and for investigating the mechanisms of therapeutic resistance [3–6].

Neuroblastoma, a childhood tumour of the developing sympathetic nervous system, remains a therapeutic challenge. Patients with high-risk tumours often have a poor prognosis despite treatment with dose-intensive chemotherapy, surgery, radiotherapy, and/or immunotherapy [7,8]. We recently established orthotopic neuroblastoma PDXs by implanting undissociated high-risk neuroblastoma fragments into the para-adrenal space of immunodeficient NOD/SCID/gamma(c)(null) (NSG) mice [9]. The neuroblastoma PDXs accurately recapitulated the genomic and phenotypic features of the corresponding patient tumours and displayed widespread and robust metastases to lungs, liver, and bone marrow. Furthermore, we established *in vitro* cultures derived from neuroblastoma PDXs, and

Abbreviations: αSMA, α-smooth muscle actin; CAFs, cancer-associated fibroblasts; ECM, extracellular matrix; huCD31, human-specific CD31; IHC, immunohistochemistry; LYVE-1, lymphatic vessel endothelial hyaluronan receptor 1; moCD34, mouse CD34; NCAM, neural cell adhesion molecule; NSG, NOD/SCID/gamma(c)(null); PDXs, patient-derived xenografts; SNP, single nucleotide polymorphism; TAMs, tumour-associated macrophages; TME, tumour microenvironment.

* Corresponding author. Tel.: +46 462226423.
E-mail address: daniel.bexell@med.lu.se (D. Bexell).

http://dx.doi.org/10.1016/j.canlet.2016.02.046
0304-3835/© 2016 The Authors. Published by Elsevier Ireland Ltd. This is an open access article under the CC BY-NC-ND license (http://creativecommons.org/licenses/by-nc-nd/4.0/).

these cells expressed neuroblastoma markers and retained tumourigenic and metastatic capacity *in vivo* after orthotopic injection into mice [9].

The undissociated tumour fragments used to establish PDX models contain both neuroblastoma cells and components of the tumour microenvironment (TME). The TME plays an important role in neuroblastoma progression and metastasis [10], tumour treatment responses, and therapeutic resistance [11,12]. Recent studies suggest that TME components can induce stem cell-like features in tumour cells [13,14]. The TME includes immune cells, cancer-associated fibroblasts (CAFs), blood vessels, lymphatic vessels, pericytes, and extracellular matrix (ECM) [15]. Aggressive neuroblastomas are typically highly vascularised with blood [16] and lymphatic [17] vessels, contain high numbers of tumour-associated macrophages (TAMs) [18,19] and CAFs [20], and are Schwannian stroma-poor tumours [21,22]. Furthermore, neuroblastomas contain lymphoid immune cells [19,23] and ECM components [24]. However, the extent to which co-engrafted human tumour stroma survives and contributes to neuroblastoma PDX growth and how murine stroma participates in this process are unknown. Therefore, and given the significance of the TME in neuroblastoma progression [10], we performed a comprehensive analysis of human and mouse stroma in neuroblastoma PDXs. Our aims were to establish: (i) whether co-engrafted patient-derived tumour stromal cells persist in neuroblastoma PDXs and (ii) examine the extent to which mouse-derived stroma replaces and reflects the TME in clinical neuroblastoma specimens.

Here we report that previously established [9] and two new PDXs (one of which lacks *MYCN* amplification) recapitulate clinically important TME hallmarks of the original neuroblastomas from patients. The rich vascularisation, pericyte coverage, TAM infiltration, and CAF and ECM composition resembled that of aggressive patient tumours. Patient-derived tumour endothelial cells were able to form blood vessels in PDXs, although tumour stroma was predominantly replaced with murine stroma. Little is known about differences in TME in different immunodeficient mouse strains. We show that the choice of mouse strain dictated the presence of TME lymphoid immune cells and lymphatic endothelial cells. Furthermore, spontaneous metastases from orthotopic neuroblastoma PDXs also contained TME components, albeit to a lesser extent than the primary tumours at the adrenal site. These results further support the use of neuroblastoma PDXs as clinically relevant models for drug testing in aggressive and metastatic neuroblastoma.

Materials & methods

Processing of viable neuroblastoma samples

Primary viable neuroblastoma samples were obtained from surgical neuroblastoma specimens. Intact tumour explants (approximately $2 \times 2 \times 2$ mm) were cryopreserved in 50% foetal bovine serum (FBS), 40% DMEM high glucose cell media (Corning, New York, USA) and 10% dimethyl sulfoxide (DMSO) by stepwise cooling using CoolCell (BioCision, Larkspur, CA, USA) and stored at –80 °C. Tumour explants were thawed immediately before implantation. The Regional Ethical Review Board at Lund University (Dnr. 2011/289) and the Ethical Committee of the Clinical Hospital of Valencia and the ISCIII (reference: B0000339 26/11/2012) approved the study. Written informed consent was obtained from patients.

Animal procedures

Animal procedures are described elsewhere [9]. Briefly, four- to six-week-old female or male NSG mice were purchased from Charles River Laboratories (Wilmington, MA, USA). Athymic nude mice were purchased from Taconic Biosciences Inc. (Hudson, NY, USA). Mice were housed under pathogen-free conditions and received autoclaved water and food. Mice were anaesthetised by 2.5% isoflurane inhalation. Intact patient-derived tumour fragments were incubated in Matrigel (BD Biosciences, San Jose, USA) for a minimum of 20 min at 4 °C before being placed in the para-adrenal space and immediately covered with Matrigel. PDX-derived cultured cells (1×10^6 cells) were injected into the adrenal gland of athymic nude mice (n = 5). Mice were sacrificed immediately when they exhibited symptoms of tumour growth. All animal procedures followed the guidelines set by the Malmö-Lund Ethical Committee for the use of laboratory animals and were conducted in accordance with the European Union directive on animal rights.

Immunohistochemistry (IHC) and histochemistry

Xenograft tumours and mice organs were formalin-fixed, embedded in paraffin, and 4 µm tissue sections were cut and analysed using single-marker IHC. A list of antibodies and their working dilutions is shown in Supplementary Table S1. Images were acquired using an Olympus BX63 microscope equipped with UPlanSApo objective lenses and a DP80 camera, and images were analysed using the cellSens Dimension imaging software (Olympus Life Sciences, Shinjuku, Japan). Slightly modified Gomori staining was used to detect reticulin fibres, Masson's trichome was used to visualise collagen type I fibres, and glycosaminoglycans were detected with Alcian blue at pH 2.5. Sections from all PDX models (n = 5) were analysed for each marker unless otherwise stated. Eight representative regions from each IHC slide (n = 1 per patient tumour/PDX) were chosen for manual quantitative analysis using cellSens Dimension. Average cell numbers were calculated for each slide and presented as the number of cells per mm^2. A quantitative analysis was performed for each ECM component in patient tumours and PDXs using Image-Pro Plus 6.0 (Media Cybernetics, Inc., Silver Spring, MD, USA).

Multi-marker IHC staining and generation of composite images

Primary antibodies were sequentially applied to the tissue. Briefly, 2 µm thick paraffin-embedded tumour sections were subjected to heat-induced epitope retrieval (HIER) in a pre-treatment module (PT-link, Dako Cytomation, Glostrup, Denmark) with Tris buffer (pH 6) before IHC staining at room temperature with an automated IHC robot (AutostainerPlus, Dako). Sections were sequentially blocked with endogenous enzyme block (EnVision™ FLEX Peroxidase-Blocking Reagent, Dako) for 10 min and serum-free protein block (Dako) for 10 min before incubation with the first primary antibodies (Supplementary Table S2) for 60 min. Next, sections were incubated with secondary antibodies for 30 min, followed by incubation with standard HRP chromogen substrate for 10 min and counterstaining with Mayer's haematoxylin. The tissue sections were then digitalised using an Olympus VS-120 virtual slide microscope (Olympus). The procedure was then repeated for the other primary antibodies (Supplementary Table S2) and the tissue sections were digitalised after each staining cycle. Finally, the new positive chromogen staining for each marker was segmented out by computerised image analysis and combined into a multi-composite marker image. Cell numbers are presented as counts.

Single nucleotide polymorphism (SNP) analysis

Patient tumours and PDXs were snap-frozen and stored at –80 °C for SNP array analysis. Briefly, DNA was extracted from the cells and tissues using the DNeasy Blood and Tissue Kit (Qiagen, Hilden, Germany) according to the manufacturer's instructions. The Affymetrix CytoScan HD platform was used for SNP array analysis as described elsewhere [9].

Results

Establishing novel neuroblastoma patient-derived orthotopic xenografts

We previously reported three metastasising neuroblastoma PDXs (PDXs #1–3) in NSG mice 59–102 days after tumour implantation [9]. Here we show successful engraftment of two additional neuroblastoma orthotopic PDXs (PDX #4–5). Tumour tissue for PDX #4 was obtained from a three-year-old child diagnosed with INSS stage III neuroblastoma who underwent surgery following chemotherapy. The SNP copy number profile (most importantly *MYCN* amplification and 17q gain; Supplementary Fig. S1A) and the neuroblastoma marker pattern (CD56/NCAM, tyrosine hydroxylase, chromogranin A, and synaptophysin; Supplementary Fig. S1B) demonstrated that the PDX retains clinically important molecular features of the corresponding patient tumour. We further used NCAM IHC to detect metastatic spread to distant organs. There were a few micrometastases in the lungs and liver (data not shown) but no evidence of macrometastatic disease and no tumour cells in the bone marrow. These findings were very similar to the clinical profile of the corresponding stage III patient, in whom no overt distant metastases were found. The metastatic behaviour of PDX #4 was different from that of the previously established stage IV tumour-derived PDXs, which showed robust distant metastatic spread [9].

Tumour tissue for PDX #5 was obtained from a three-year-old child with INSS stage IV neuroblastoma that harboured 1p del(etion), 17q gain, and other chromosomal changes including 1pq gain, 2p gain, 4p del, complex chromothripsis-like structural aberrations on chromosome 5, 6p gain, 9pq del, 14q del, and 18q gain but no *MYCN* amplification (Supplementary Fig. S2A). Most of the chromosomal aberrations, including 1p del and 17q gain, were retained in PDX #5 (Supplementary Fig. S2A). There were a few genetic differences between the patient sample and the PDX including 8q del in the PDX (Supplementary Fig. S2A). PDX #5 also retained the expression of neuroblastoma markers CD56/NCAM, tyrosine hydroxylase, chromogranin A, and synaptophysin (Supplementary Fig. S2B) and displayed significant metastatic spread to lungs and liver (Supplementary Fig. S2C), but there was no evidence of bone marrow involvement. PDX #5 represents the first non-*MYCN* amplified metastatic neuroblastoma PDX derived from a high-stage tumour.

Immune cell distribution in neuroblastoma PDXs

We next investigated neuroblastoma TME hallmarks in the five PDXs. The TME was assessed in PDXs established by implantation of patient-derived undissociated tumour pieces unless otherwise stated.

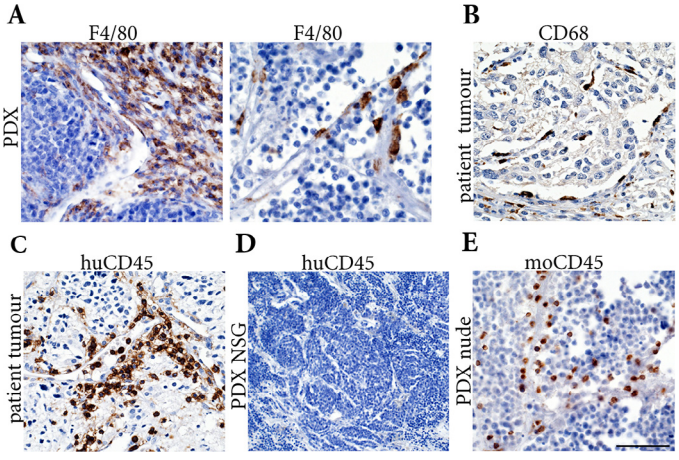

Fig. 1. Distribution of immune cells in neuroblastoma PDXs. F4/80-expressing mouse tumour-associated macrophages (TAMs) in neuroblastoma PDXs located in cohesive clusters or the perivascular niche, exemplified by PDX #1 (A). CD68-positive human TAMs in the perivascular niche of a patient sample (B). Human CD45+ lymphoid cells in a patient sample (C). Lack of human CD45-expressing cells in neuroblastoma PDXs grown in NSG mice (D). Mouse CD45-expressing lymphoid immune cells in neuroblastoma PDXs grown in athymic nude mice, exemplified by PDX #2 (E). Scale bar: 50 μm for A–C, E and 150 μm for D.

We first examined the intratumoural distribution of immune cells. Mouse F4/80-expressing TAMs infiltrated all five neuroblastoma PDXs (Supplementary Table S3A). TAMs were distributed either as cohesive cell clusters in stromal regions or as single scattered cells located in the perivascular niche (Fig. 1A). As expected, there was no F4/80 positivity in patient samples (data not shown). The human-specific monocyte/macrophage marker CD68 was used to detect human TAMs. CD68+ TAMs were found in patient samples, often in the perivascular niche (Fig. 1B), but PDXs were negative for these cells (data not shown).

We next examined if human lymphoid cells co-engraft in neuroblastoma PDXs established by implantation of undissociated tumour fragments into NSG mice. Human-specific CD45-positive lymphoid cells were found in human tonsil tissue (used as a positive control, data not shown) and in patient samples (Fig. 1C). There was no evidence of human CD45-expressing lymphoid cells in PDXs (Fig. 1D) or in the spleens of mice carrying PDXs (data not shown). However, mouse-specific anti-CD45 antibodies detected lymphoid cells in tumours established by orthotopic injection of cultured PDX-derived cells into athymic nude mice (Fig. 1E, Supplementary Table S3A).

Mouse CAFs infiltrate PDXs

Staining with an anti-vimentin mouse/human antibody revealed large numbers of positive cells in all five PDXs (Fig. 2A). These cells had a spindle-shaped morphology and were distributed either as single scattered cells interspersed between tumour cells or as cohesive clusters in thick bands of fibrous stroma, consistent with CAFs. We next examined if co-engrafted human CAFs survive in neuroblastoma PDXs using a human-specific anti-vimentin antibody. Patient samples served as positive controls (Fig. 2B). Analysis of consecutive PDX sections revealed several areas containing large numbers of mouse/human vimentin-positive cells co-expressing α-smooth muscle actin (αSMA) and lacking expression of human-specific vimentin (Fig. 2C). Quantitative data are presented in Supplementary Table S3A. We concluded that mouse but not human CAFs contribute to the stromal compartment of neuroblastoma PDXs.

Aggressive neuroblastomas are typically Schwannian stroma-poor tumours. Antibodies targeting human and mouse S-100β and mouse myelin revealed no evidence of S-100β- or mouse myelin-positive cells in neuroblastoma PDXs.

Neuroblastoma PDXs reflect the angiogenic profile of patient tumours

PDXs #1–5 were vascularised and contained numerous mouse CD34 (moCD34)-expressing endothelial cells (Fig. 3A, Supplementary Table S3A). A human-specific CD31 (huCD31) antibody was used to detect human-derived endothelial cells. As expected, there were large numbers of huCD31+ endothelial cells in patient samples (Fig. 3B)

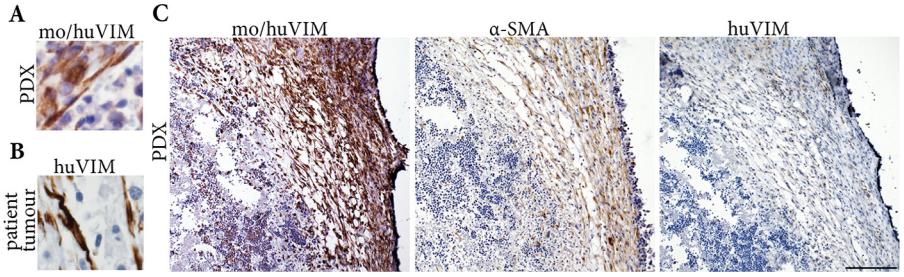

Fig. 2. Cancer-associated fibroblasts (CAFs) contribute to neuroblastoma PDX stroma. Spindle-shaped CAFs expressing mouse/human vimentin in neuroblastoma PDXs, exemplified by PDX #3 (A). Vimentin-expressing human CAFs in a patient sample (B). Expression of mouse/human vimentin, α-smooth muscle actin, and lack of human-specific vimentin in consecutive sections of PDX #3 (C). Scale bar: 30 μm for A, B and 200 μm for C.

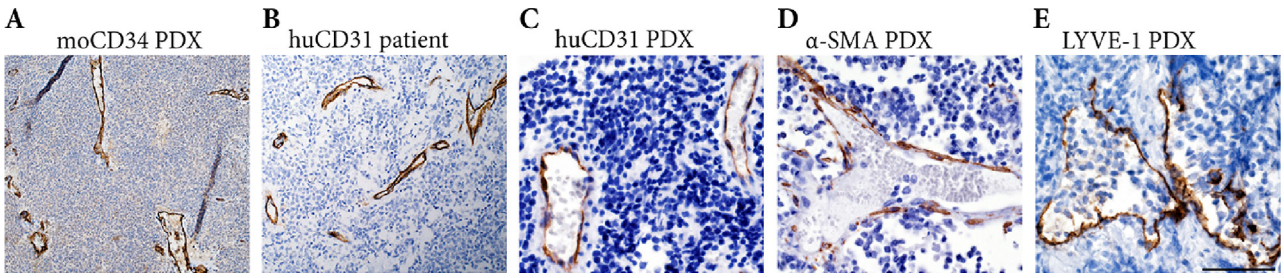

Fig. 3. Neuroblastoma PDXs retain the vascular profile of patient tumours. Mouse CD34+ tumour endothelial cells in PDX #4 (A). Human CD31+ endothelial cells in a patient sample (B). Patient-derived human CD31+ endothelial cells in PDX #4 (C). Alpha-smooth muscle actin-expressing pericytes in PDXs, exemplified by PDX #1 (D). Intratumoural LYVE-1-expressing lymphatic vessels in a PDX grown in an athymic nude mouse, exemplified by PDX #2 (E). Scale bar: 150 μm for A, B and 70 μm for C–E.

and also several huCD31+ cells in the 1st in *vivo* generation PDXs #4 and #5. These huCD31+ cells had a thin and elongated morphology and delineated blood vessels, demonstrating their endothelial nature (Fig. 3C). Intratumoural human endothelial cells decreased significantly after *in vivo* passage to secondary recipients. The other three PDX models (#1–3) lacked huCD31-expressing cells.

Alpha-smooth muscle actin (α-SMA)-expressing pericytes/smooth muscle cells supported the blood vessels in all five PDXs (Fig. 3D). We further analysed lymphatic vessel distribution in neuroblastoma PDXs using the mouse-specific LYVE-1 antibody, which binds to hyaluronan receptors on lymphatic vessel walls [25]. Numerous LYVE-1 positive lymphatic endothelial cells were observed in athymic nude mice carrying cultured PDX cell-derived tumours (Fig. 3E). The central regions of PDXs mostly contained collapsed lymphatic vessels, while the peripheral parts of the tumours contained larger lymph vessels with open lumina. There was no evidence of lymphatic vessels in tumour-bearing NSG mice (data not shown).

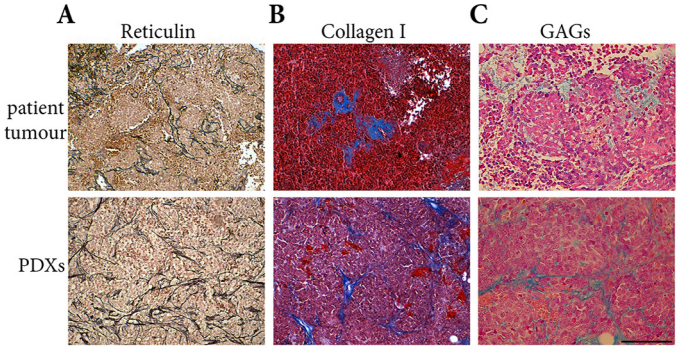

Fig. 4. Neuroblastoma PDXs resemble extracellular matrix components of aggressive patient tumours. Reticulin fibres in a high-risk patient tumour and in PDX #1 visualised with Gomori staining (A). Thick bundles of perivascular type I collagen fibres (Masson's trichrome, blue, B), and glycosaminoglycans (Alcian blue, light blue, C) in a high-risk patient tumour and in PDX #2. Scale bar: 100 μm for A, B and 50 μm for C. (For interpretation of the references to colour in this figure legend, the reader is referred to the web version of this article.)

The ECM composition of neuroblastoma PDXs resembles that of aggressive patient tumours

The ECM of aggressive human neuroblastomas contains abundant reticulin fibres and a few collagen type I fibres and glycosaminoglycans [24]. Similarly, reticulin fibres, collagen type I fibres restricted to blood vessels, and glycosaminoglycans were found in PDXs (Fig. 4, Supplementary Table S3B). Thus, the ECM of neuroblastoma PDXs reflects the ECM profile of aggressive human neuroblastomas.

Distribution of stromal cells at metastatic sites

Neuroblastoma PDXs #1–3 have been shown to metastasise spontaneously to distant organs [9]. Here, we investigated the stromal cell composition in metastatic liver lesions from PDXs #1–3. NCAM, which is expressed by virtually all neuroblastoma PDX cells [9], was used to identify metastatic neuroblastoma cells in the liver. The high density of NCAM-expressing cells without significant stroma suggested that stroma was less abundant in metastatic liver lesions compared to primary tumours (Fig. 5A). Indeed, metastatic lesions only contained a few CD34-expressing endothelial cells (Fig. 5B), α-SMA-expressing pericytes (Fig. 5C), and vimentin-expressing CAFs (Fig. 5D).

Orthotopic neuroblastomas derived from cultured PDX cells retain microenvironmental hallmarks

As shown above, neuroblastomas established by orthotopic injection of cultured PDX cells into athymic nude mice contain mouse CD45+ lymphoid cells (Fig. 1E) and mouse lymphatic vessels (Fig. 3E). Further analysis of these tumours showed that they also retained the other important TME hallmarks with rich vascularisation, pericyte coverage, CAFs, and TAM infiltration (Supplementary Fig. S3).

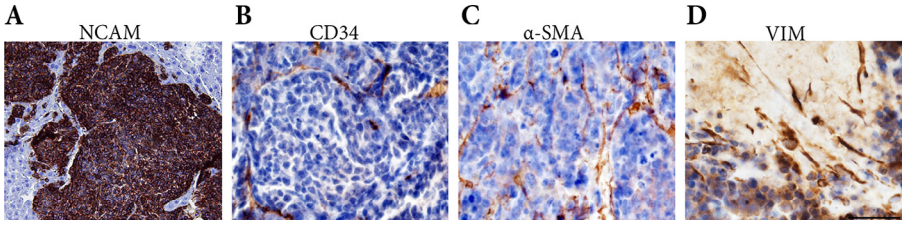

Fig. 5. The tumour microenvironment of neuroblastoma metastases. Neuroblastoma PDX liver metastasis identified by NCAM expression (A). CD34+ mouse endothelial cells (B), α-smooth muscle actin-expressing pericytes (C), and vimentin-expressing CAFs (D) in a neuroblastoma PDX liver metastasis. Scale bar: 130 μm in A and 50 μm in B–D.

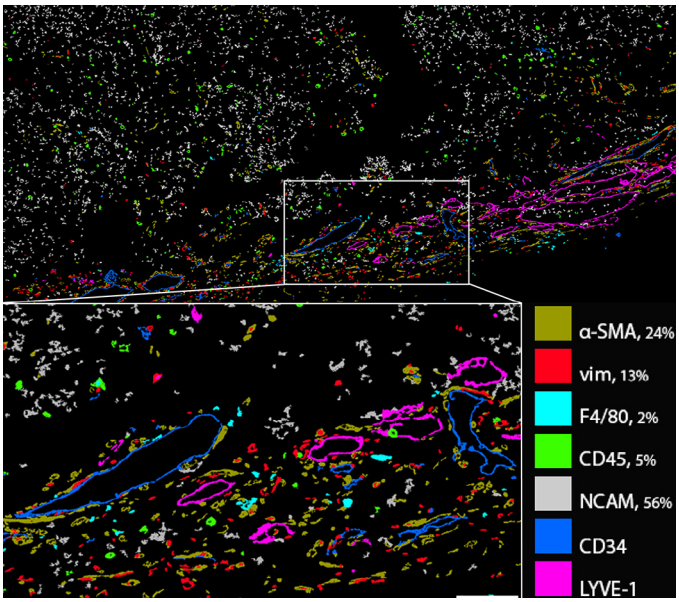

Fig. 6. Integrated overview of tumour and stromal cells in a neuroblastoma orthotopic PDX. Multi-composite image revealing an integrated view of the PDX tumour microenvironment and the well retained structural and cellular complexity similar to the patient tumour. The upper panel shows a stroma-poor region with densely packed NCAM+ neuroblastoma cells admixed with single scattered stromal cells. Relative numbers of the different cell types are shown in the upper panel. The magnified peripheral part of the tumour (lower panel) shows a stroma-rich region with few NCAM-positive tumour cells and a large number of several different stromal cell types. Scale bar is 150 μm in the upper panel and 50 μm in the lower panel. (For interpretation of the references to colour in this figure legend, the reader is referred to the web version of this article.)

Integrated overview of tumour and stromal cells in neuroblastoma PDXs

Finally, a multi-marker IHC approach was used to provide a single composite image of seven different cell types in a neuroblastoma PDX grown in an athymic nude mouse. Antibodies against mouse α-SMA, mouse vimentin, mouse F4/80, mouse CD45, NCAM, CD34, and LYVE-1 were used. Single antibody staining of these markers is presented in Supplementary Fig. S1 and Figs. 1–4. Neuroblastoma PDXs contained large areas of densely packed NCAM+ tumour cells with only single scattered stromal cells. Areas with a high density of stromal cells were heterogeneous in PDXs and were often located in peripheral parts of the tumour (Fig. 6). Using automatic image-based quantitative analysis of a stroma-rich area, we estimated the relative amounts of the different cell types (excluding blood and lymphatic vessels; see Fig. 6). However, although indicative of composite cell numbers, the automatic analysis could potentially overestimate or underestimate the actual cell numbers due to cell fragmentation or clustering in the images.

Discussion

Patient-derived xenografts (PDXs) are promising models for oncology preclinical drug testing because they are more predictive of clinical outcome than conventional cell line-derived xenografts [3,4,6]. We recently established a set of invasive and metastasising neuroblastoma orthotopic PDXs containing tumour cells that retained the genotypes and phenotypes of their corresponding patient tumours [9]. Here, we established two additional neuroblastoma orthotopic PDX models: an *MYCN*-amplified PDX (#4) derived from a stage III tumour with minimal metastatic spread and a metastatic PDX (#5) derived from a non-*MYCN*-amplified stage IV tumour. Interestingly, the PDX established from the stage III tumour did not metastasise to the same extent as PDXs established from stage IV tumours, thus closely mimicking this important clinical feature of the tumour from which it was derived. Neuroblastoma PDXs were found to contain rich blood vessel vascularisation, pericyte coverage, TAMs, CAFs, and ECM components resembling the TME hallmarks of aggressive neuroblastomas. In addition, lymphoid cells and lymphatic vessels were present in PDXs grown in athymic nude mice but not in NSG mice. Two neuroblastoma PDX models contained patient-derived tumour endothelial cells that formed tumour vasculature; however, the human stroma in these tumours was replaced by mouse stroma during *in vivo* passaging. The distant tumour metastases also contained TME hallmarks but to a lesser extent than the primary tumours.

The presence of infiltrating TAMs in PDXs is in agreement with the positive association of TAMs with the metastatic phenotype in neuroblastoma patients [18]. The blood and lymphatic vascularisation in neuroblastoma PDXs resembled the vascular profile of clinical neuroblastomas [16,26]. The presence of collapsed lymphatic vessels in central regions and larger lymphatic vessels in the periphery was also consistent with the histopathological findings of clinical neuroblastomas [26]. The observation that the majority of stromal cells in PDXs were CAFs, either scattered among tumour cells or as thick bands of fibrous stroma, was another striking similarity with clinical samples [20]. However, the number of PDX stromal cells was generally lower than in their corresponding patient tumours. Furthermore, the function of murine stroma in PDXs remains largely unknown. Some stroma-derived growth factors such as TNF may not be cross-reactive between species [27], and it will be important to clarify the functional significance of murine stroma in treatment responses and resistance in neuroblastoma PDXs.

The finding that patient-derived tumour endothelial cells can form tumour vasculature opens up the possibility of studying and targeting human neuroblastoma–tumour vasculature interactions *in vivo*. However, since mouse endothelium replaced human vessels after two passages *in vivo*, it will be important to develop methods that increase the survival and integration of human TME components in PDXs, especially when testing species-specific anticancer compounds that target the tumour stroma. One possibility would be to co-inject human stromal components (e.g., human endothelial cells or mesenchymal stem cells [28]) with patient-derived tumour cells. While co-engraftment of patient-derived endothelial cells is in agreement with findings from prostate cancer primary xenografts [29], the absence of patient-derived immune cells in our PDXs differs from the findings in other PDX models [30,31].

There were also differences between athymic nude mice (with defective T cell function) and severely immunodeficient NSG mice (lacking functional T-, B-, and NK cells), which created different TMEs. Neuroblastoma PDXs in nude mice contained mouse intratumoural lymphatic vessels and mouse CD45+ lymphoid cells in the perivascular niche while NSG mice lacked these components. Given the important role of lymphoid cells and lymphatic vessels in tumour progression and metastasis [32,33], these differences must be considered when designing preclinical drug testing protocols using PDXs. The lack of a proper immune system in immunodeficient mice is, of course, a limitation for the development of immunotherapies; however, reconstitution of the human immune system in immunodeficient mice could make PDXs suitable for this application [34–37].

In conclusion, neuroblastoma PDXs retain clinically important TME hallmarks of aggressive and metastatic clinical neuroblastomas including rich tumour blood and lymphatic vascularisation, pericyte coverage, TAM and lymphoid cell infiltration, CAFs, and ECM components. Patient-derived endothelial cells have the capacity to form tumour blood vessels but murine stroma largely replaces the human TME; therefore, strategies to faithfully reconstitute the human

TME in PDXs might be necessary to further improve these models for human tumour–TME interaction studies *in vivo*. Many of the TME components found in neuroblastoma PDXs are implicated as crucial mediators of tumour growth, metastasis, and therapeutic responses and resistance [10–12,18,32,33]. Our findings further support the use of orthotopic neuroblastoma PDXs as clinically relevant models for drug testing of metastatic neuroblastoma.

Acknowledgements

This work was supported by grants from the Swedish Cancer Society, Swedish Childhood Cancer Foundation, the Swedish Research Council, VINNOVA, the SSF Strategic Center for Translational Cancer Research-CREATE Health, the Strategic Cancer Research Program BioCARE, Crafoord Foundation, Jeanssons Stiftelser, Berth von Kantzows Stiftelse, Royal Physiographic Society in Lund, Gunnar Nilsson Cancer Foundation, The Gyllenstierna Krapperup's Foundation, Ollie och Elof Ericssons Stiftelser, Region Skåne, Skåne University Hospital research funds, and grants from the FIS contract PI14/01008, RTICC contracts RD12/0036/0027, and the ISCIII & FEDER (European Regional Development Fund), Spain.

Conflict of interest

JSE is the owner of Medetect AB. CS and JJ are employed by Medetect AB. The other co-authors have no conflict of interest.

Appendix: Supplementary material

Supplementary data to this article can be found online at doi:10.1016/j.canlet.2016.02.046.

References

[1] I. Kola, J. Landis, Can the pharmaceutical industry reduce attrition rates?, Nat. Rev. Drug Discov. 3 (2004) 711–715.
[2] A. Ocana, A. Pandiella, L.L. Siu, I.F. Tannock, Preclinical development of molecular-targeted agents for cancer, Nat. Rev. Clin. Oncol. 8 (2011) 200–209.
[3] M. Hidalgo, F. Amant, A.V. Biankin, E. Budinska, A.T. Byrne, C. Caldas, et al., Patient-derived xenograft models: an emerging platform for translational cancer research, Cancer Discov. 4 (2014) 998–1013.
[4] J.J. Tentler, A.C. Tan, C.D. Weekes, A. Jimeno, S. Leong, T.M. Pitts, et al., Patient-derived tumour xenografts as models for oncology drug development, Nat. Rev. Clin. Oncol. 9 (2012) 338–350.
[5] D. Siolas, G.J. Hannon, Patient-derived tumor xenografts: transforming clinical samples into mouse models, Cancer Res. 73 (2013) 5315–5319.
[6] E. Rosfjord, J. Lucas, G. Li, H.P. Gerber, Advances in patient-derived tumor xenografts: from target identification to predicting clinical response rates in oncology, Biochem. Pharmacol. 91 (2014) 135–143.
[7] N.K. Cheung, M.A. Dyer, Neuroblastoma: developmental biology, cancer genomics and immunotherapy, Nat. Rev. Cancer 13 (2013) 397–411.
[8] J.M. Maris, M.D. Hogarty, R. Bagatell, S.L. Cohn, Neuroblastoma, Lancet 369 (2007) 2106–2120.
[9] N. Braekeveldt, C. Wigerup, D. Gisselsson, S. Mohlin, M. Merselius, S. Beckman, et al., Neuroblastoma patient-derived orthotopic xenografts retain metastatic patterns and geno- and phenotypes of patient tumours, Int. J. Cancer 136 (2015) E252–E261.
[10] L. Borriello, R.C. Seeger, S. Asgharzadeh, Y.A. DeClerck, More than the genes, the tumor microenvironment in neuroblastoma, Cancer Lett. (2015), doi:10.1016/j.canlet.2015.11.017.
[11] F. Klemm, J.A. Joyce, Microenvironmental regulation of therapeutic response in cancer, Trends Cell Biol. 25 (2015) 198–213.
[12] H.E. Barker, J.T. Paget, A.A. Khan, K.J. Harrington, The tumour microenvironment after radiotherapy: mechanisms of resistance and recurrence, Nat. Rev. Cancer 15 (2015) 409–425.
[13] N. Charles, T. Ozawa, M. Squatrito, A.M. Bleau, C.W. Brennan, D. Hambardzumyan, et al., Perivascular nitric oxide activates notch signaling and promotes stem-like character in PDGF-induced glioma cells, Cell Stem Cell 6 (2010) 141–152.
[14] L. Vermeulen, E.M.F. De Sousa, M. van der Heijden, K. Cameron, J.H. de Jong, T. Borovski, et al., Wnt activity defines colon cancer stem cells and is regulated by the microenvironment, Nat. Cell Biol. 12 (2010) 468–476.
[15] K. Pietras, A. Ostman, Hallmarks of cancer: interactions with the tumor stroma, Exp. Cell Res. 316 (2010) 1324–1331.
[16] D. Meitar, S.E. Crawford, A.W. Rademaker, S.L. Cohn, Tumor angiogenesis correlates with metastatic disease, N-myc amplification, and poor outcome in human neuroblastoma, J. Clin. Oncol. 14 (1996) 405–414.
[17] D. Ribatti, B. Nico, A.M. Cimpean, M. Raica, Podoplanin and LYVE-1 expression in lymphatic vessels of human neuroblastoma, J. Neurooncol. 100 (2010) 151–152.
[18] S. Asgharzadeh, J.A. Salo, L. Ji, A. Oberthuer, M. Fischer, F. Berthold, et al., Clinical significance of tumor-associated inflammatory cells in metastatic neuroblastoma, J. Clin. Oncol. 30 (2012) 3525–3532.
[19] J. Vakkila, R. Jaffe, M. Michelow, M.T. Lotze, Pediatric cancers are infiltrated predominantly by macrophages and contain a paucity of dendritic cells: a major nosologic difference with adult tumors, Clin. Cancer Res. 12 (2006) 2049–2054.
[20] R. Zeine, H.R. Salwen, R. Peddinti, Y. Tian, L. Guerrero, Q. Yang, et al., Presence of cancer-associated fibroblasts inversely correlates with Schwannian stroma in neuroblastoma tumors, Mod. Pathol. 22 (2009) 950–958.
[21] H. Shimada, I.M. Ambros, L.P. Dehner, J. Hata, V.V. Joshi, B. Roald, et al., The International Neuroblastoma Pathology Classification (the Shimada system), Cancer 86 (1999) 364–372.
[22] H. Shimada, J. Chatten, W.A. Newton Jr., N. Sachs, A.B. Hamoudi, T. Chiba, et al., Histopathologic prognostic factors in neuroblastic tumors: definition of subtypes of ganglioneuroblastoma and an age-linked classification of neuroblastomas, J. Natl. Cancer Inst. 73 (1984) 405–416.
[23] A.P. Berbegall, E. Villamon, I. Tadeo, T. Martinsson, A. Canete, V. Castel, et al., Neuroblastoma after childhood: prognostic relevance of segmental chromosome aberrations, ATRX protein status, and immune cell infiltration, Neoplasia 16 (2014) 471–480.
[24] I. Tadeo, M. Piqueras, D. Montaner, E. Villamon, A.P. Berbegall, A. Canete, et al., Quantitative modeling of clinical, cellular, and extracellular matrix variables suggest prognostic indicators in cancer: a model in neuroblastoma, Pediatr. Res. 75 (2014) 302–314.
[25] D.G. Jackson, The lymphatics revisited: new perspectives from the hyaluronan receptor LYVE-1, Trends Cardiovasc. Med. 13 (2003) 1–7.
[26] P. Ramani, J.V. Dungwa, M.T. May, LYVE-1 upregulation and lymphatic invasion correlate with adverse prognostic factors and lymph node metastasis in neuroblastoma, Virchows Arch. 460 (2012) 183–191.
[27] C. Bossen, K. Ingold, A. Tardivel, J.L. Bodmer, O. Gaide, S. Hertig, et al., Interactions of tumor necrosis factor (TNF) and TNF receptor family members in the mouse and human, J. Biol. Chem. 281 (2006) 13964–13971.
[28] Y.S. DeRose, G. Wang, Y.C. Lin, P.S. Bernard, S.S. Buys, M.T. Ebbert, et al., Tumor grafts derived from women with breast cancer authentically reflect tumor pathology, growth, metastasis and disease outcomes, Nat. Med. 17 (2011) 1514–1520.
[29] D.R. Gray, W.J. Huss, J.M. Yau, L.E. Durham, E.S. Werdin, W.K. Funkhouser Jr., et al., Short-term human prostate primary xenografts: an in vivo model of human prostate cancer vasculature and angiogenesis, Cancer Res. 64 (2004) 1712–1721.
[30] R.B. Bankert, S.V. Balu-Iyer, K. Odunsi, L.D. Shultz, R.J. Kelleher Jr., J.L. Barnas, et al., Humanized mouse model of ovarian cancer recapitulates patient solid tumor progression, ascites formation, and metastasis, PLoS ONE 6 (2011) e24420.
[31] M.R. Simpson-Abelson, G.F. Sonnenberg, H. Takita, S.J. Yokota, T.F. Conway Jr., R.J. Kelleher Jr., et al., Long-term engraftment and expansion of tumor-derived memory T cells following the implantation of non-disrupted pieces of human lung tumor into NOD-scid IL2Rgamma(null) mice, J. Immunol. 180 (2008) 7009–7018.
[32] D. Hanahan, R.A. Weinberg, Hallmarks of cancer: the next generation, Cell 144 (2011) 646–674.
[33] S. Karaman, M. Detmar, Mechanisms of lymphatic metastasis, J. Clin. Invest. 124 (2014) 922–928.
[34] A.K. Wege, W. Ernst, J. Eckl, B. Frankenberger, A. Vollmann-Zwerenz, D.N. Mannel, et al., Humanized tumor mice – a new model to study and manipulate the immune response in advanced cancer therapy, Int. J. Cancer 129 (2011) 2194–2206.
[35] D. Liu, L. Song, J. Wei, A.N. Courtney, X. Gao, E. Marinova, et al., IL-15 protects NKT cells from inhibition by tumor-associated macrophages and enhances antimetastatic activity, J. Clin. Invest. 122 (2012) 2221–2233.
[36] A. Rongvaux, T. Willinger, J. Martinek, T. Strowig, S.V. Gearty, L.L. Teichmann, et al., Development and function of human innate immune cells in a humanized mouse model, Nat. Biotechnol. 32 (2014) 364–372.
[37] J.J. Morton, G. Bird, S.B. Keysar, D.P. Astling, T.R. Lyons, R.T. Anderson, et al., XactMice: humanizing mouse bone marrow enables microenvironment reconstitution in a patient-derived xenograft model of head and neck cancer, Oncogene 35 (2016) 290–300.